Available online at www.sciencedirect.com
ScienceDirect
Polymer 49 (2008) 1981–1992
polymer
www.elsevier.com/locate/polymer

Monte Carlo simulation of two interpenetrating polymer networks: Structure, swelling, and mechanical properties

Samuel Edgecombe, Per Linse*

Physical Chemistry 1, Center for Chemistry and Chemical Engineering, Lund University, P.O. Box 124, S-221 00 Lund, Sweden

Received 17 December 2007; received in revised form 9 February 2008; accepted 11 February 2008
Available online 16 February 2008

Abstract

The swelling and mechanical properties of various interpenetrating polymer networks (IPNs) were studied. Six networks made from permutations of a moderately crosslinked polyelectrolyte network (ref), a moderately crosslinked neutral polymer network (net1), and a highly crosslinked polyelectrolyte network (net2) were first swollen in water and structural properties such as end-to-end chain lengths and radial distribution functions were compared with the component networks' equilibrium properties. The swelling of composite IPNs was discussed in terms of a balance between the osmotic pressure due to mobile counterions and the restoring force of the network chains, which act in parallel to counteract the osmotic swelling. For the ref–net2 system, the strong stretching of net2 chains increases the network restoring force and the further swelling due to the counterions is suppressed. The swollen networks were then uniaxially stretched, and equilibrium stress–strain plots were obtained up to high extension ratios. The equilibrium volume decreased upon uniaxial extension, and the elastic moduli of IPNs of the A–A type were slightly greater than that of their respective single networks.

Keywords: Interpenetrating polymer networks; Static properties; Monte Carlo simulation

1. Introduction

Polyelectrolyte gels have received considerable interest in recent years due to their exceptional swelling properties. One problem with polyelectrolyte gels is that highly swollen gels have relatively poor mechanical properties. One way to overcome this problem is to make a gel composed of two interpenetrating networks by crosslinking a polymer (or polyelectrolyte) (Polymer II) into a pre-existing highly crosslinked network of a polymer (or polyelectrolyte) (Polymer I) of a different kind. Gong and coworkers have confirmed that such interpenetrating networks have increased elastic and mechanical properties by measuring the stress–strain behavior of a number of interpenetrating networks and comparing their elastic moduli and breaking points [1–5]. Independently, work by Myung et al. has also demonstrated the same phenomenon [6,7]. In Gong's group, they have worked on interpenetrating a network of one loosely crosslinked polymer network, poly(acrylamide) (PAAm), into a highly crosslinked charged network, poly(2-acrylamido-2-methylpropanesulfonic acid) (PAMPS). Myung et al. have focused on interpenetrating a network of one loosely crosslinked polyelectrolyte network, poly(acrylic acid) (PAA), into a highly crosslinked neutral network, poly(ethylene glycol) (PEG). Interpenetrating networks are already being tested for use in applications such as cartilage [8] and cornea replacement [6,9], utilising their properties of increased wear resistance and improved elastic moduli, respectively.

When discussing the enhanced mechanical properties of the gels, we can distinguish between (i) the increase in elastic modulus (increased stiffness) and (ii) the increased strain at which networks physically break. The first observation has been proposed due to the presence of a stiff Polymer I network, as the initial gradients of the stress–strain curves for a single PAMPS and an interpenetrating PAMPS–PAAm network overlap [1]. Observation (ii) is thought to be due to the increased

* Corresponding author.
E-mail address: per.linse@fkem1.lu.se (P. Linse).

0032-3861/$ - see front matter © 2008 Elsevier Ltd. All rights reserved.
doi:10.1016/j.polymer.2008.02.018

effective fracture energy when the broken Polymer II network chains entangle with the loose Polymer I chains [10].

Whereas experiments on interpenetrating networks are new, but not uncommon, there is little theoretical work done on such systems. Uniaxial extension simulations on single polymer networks have been performed [11,12] and also on interpenetrating diamond networks at melt density [13]. More recently one swollen poly(ethylene oxide)–poly(acrylic acid) (PEO–PAA) interpenetrating network has been simulated by Goddard and coworkers where mechanical and transport properties were calculated [14]. Observation (i) was also seen in their simulations and was attributed to the strong stretching of the short PEO chains which were stretched as compared to their corresponding single network.

In this contribution, we systematically study a range of single polymer networks and double interpenetrating polymer networks of the diamond type to examine the swelling, structure, and mechanical properties as a function of polymer charge and crosslinking density of such networks. Our main conclusion confirms observation (i) that the increased elastic modulus appearing in double interpenetrating networks arises mainly due to the strong stretching of Polymer I.

2. Model

2.1. General properties

A coarse-grained approach based on the primitive model of electrolytes has been used to describe polyelectrolyte gels. We have adopted basically the same model as in previous studies of polyelectrolyte gels from our laboratory [15–18].

In the most general case, a system is composed of two interpenetrating positively charged networks and negatively charged counterions dissolved in excess of water. A network is composed of chains that are end-connected to tetrafunctional crosslinkers (nodes). The chains consist of spheres (beads) that are connected by springs. The topology of a single network is diamond-like (see Fig. 1), and this topology is conserved during the simulation. Beads and nodes will collectively be referred to as network particles. Network particles and counterions are treated as charged Lennard-Jones (LJ) spheres. The particles of a network carry the same charge $z_{\text{bead}} = z_{\text{node}}$ and possess the same LJ diameter $\sigma_{\text{bead}} = \sigma_{\text{node}} = 2$ Å. The number of beads per chain is denoted by n_{bead}, and all chains are fully flexible. There are n_{ion} counterions with diameter $\sigma_{\text{ion}} = 2$ Å, compensating the net charge of the network. The solvent is modeled as a homogeneous dielectric continuum. General data of the model are collected in Table 1.

2.2. Potential energy

The potential energy U of a system can be expressed as a sum of three energy terms according to

$$U = U_{\text{LJ}} + U_{\text{elec}} + U_{\text{bond}} \tag{1}$$

The LJ potential energy U_{LJ} is given by

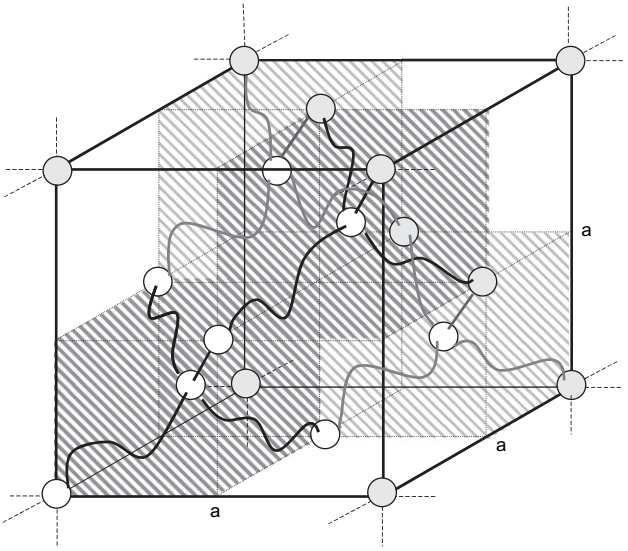

Fig. 1. Schematic illustration of one unit cell of a defect-free network of diamond-like topology containing eight tetrafunctional nodes (spheres) linked by non-crossing chains (wavy lines). Note that four of the eight subcubes contain chains (shaded) whereas the other four are empty.

Table 1
General data of the model

Node diameter	σ_{node}	2 Å
Node charge	z_{node}	0 and +1
Bead diameter	σ_{bead}	2 Å
Bead charge	z_{bead}	0 and +1
Counterion diameter	σ_{ion}	2 Å
Counterion charge	z_{ion}	−1
No. of beads per chain	n_{bead}	20 and 10
Temperature	T	298 K
Relative permittivity	ϵ_{r}	80

$$U_{\text{LJ}} = \sum_{i<j} u_{ij}^{\text{LJ}}(r_{ij}) \tag{2}$$

where

$$u_{ij}^{\text{LJ}}(r_{ij}) = \begin{cases} 4\epsilon\left[(r/\sigma)^{12} - (r/\sigma)^{6}\right] + \epsilon & \text{if } r_{ij} < 2^{1/6}\sigma \\ 0 & \text{if } r_{ij} \geq 2^{1/6}\sigma \end{cases}$$

with σ denoting the LJ diameter of particle i (node, bead, or counterion), $\epsilon = 1k_{\text{B}}T$, and $r_{ij} = |\mathbf{r}_i - \mathbf{r}_j|$ the center-to-center distance between two particles. Hence, we are using a LJ potential truncated at $R_{\text{cut}} = 2^{1/6}\sigma$ and shifted by ϵ to make the potential continuous at R_{cut}, resulting in a short-range repulsive potential. The electrostatic potential energy U_{elec} is given according to

$$U_{\text{elec}} = \sum_{i<j} \frac{z_i z_j e^2}{4\pi\epsilon_0\epsilon_{\text{r}} r_{ij}} \tag{3}$$

where z_i is the valence of particle i, e the elementary charge, ϵ_0 the permittivity of vacuum, and ϵ_{r} the relative permittivity

Table 2
Specification of networks

Network	z_{node}	z_{bead}	n_{bead}
ref	+1	+1	20
net1	0	0	20
net2	+1	+1	10

of the solvent. The harmonic bond potential energy U_{bond} is given by

$$U_{bond} = \sum_{m=1}^{N_{bond}} \frac{k_{bond}}{2}(r_m - r_0)^2 \quad (4)$$

where N_{bond} is the number of bonds in the network (node–bead and bead–bead bonds), r_m the length of bond m, $r_0 = 5$ Å the unperturbed equilibrium distance, and $k_{bond} = 0.4$ N/m the bond force constant. When all interactions are considered, the root-mean-square (rms) bead-to-bead separation $\langle R_{bb}^2 \rangle^{1/2}$ ranges from 5.5 to 6.0 Å.

2.3. Systems

We will examine nine different systems, three single networks and six having two interpenetrating networks. One of the networks is referred to as the reference network (ref) and is characterized by (i) monovalent node and bead charges, $z_{node} = z_{bead} = +1$, and (ii) a chain length $n_{bead} = 20$. As compared to the reference network, the second network (net1) has no charge, $z_{node} = z_{bead} = 0$, and hence has no associated counterions, and the third network (net2) has shorter chains, $n_{bead} = 10$ (see also Table 2). The six systems having two interpenetrating networks were constructed by combining the three different networks. These systems will be referred to as A–B, where A and B is either ref, net1, or net2.

3. Simulation details

Monte Carlo simulations were performed using the *NVT* (constant number of particles, constant volume, and constant temperature) ensemble employing the Metropolis algorithm [19]. The particles were enclosed in a cubic box of length L, and periodic boundary conditions were applied. The long-range nature of the Coulomb interaction was handled by using the Ewald summation with conducting boundary conditions. Volumes and mechanical properties were determined by using systems comprising one unit cell, whereas structural properties were obtained from simulations with eight unit cells. One unit cell contained $N_{node} = 8$ nodes and $N_{chain} = 16$ chains per network.

Single particles were subjected to trial translational displacements ranging from 2.5 (network particles) to 10 Å (counterions). The displacements of network particles were small enough to preserve the network topology. The equilibration runs involved at least 10^4 passes (trial moves per particle) and the production runs at least 10^5 passes. The uncertainty of ensemble averages was estimated from 10 block averages. All simulations were performed using the integrated molecular dynamics/Monte Carlo/Brownian dynamics package MOLSIM [20].

The osmotic pressure of the gel was evaluated as the sum of the ideal and a virial term [18]. If nothing else is stated, the results are given at zero osmotic pressure corresponding to the condition that the gel is in equilibrium with pure water. The volume of the gel in equilibrium with pure water was obtained from simulated pressure–volume isotherms at zero osmotic pressure.

4. Results and discussion

4.1. Swelling

The swelling behavior as expressed by the volume per unit cell of the nine different systems with either a single network or two interpenetrating networks at equilibrium with pure water will now be considered. Connected to this discussion is also the fraction of counterions associated to the network, $f_{ion}^{ass} = n_{ion}^{ass}/n_{ion}$, where n_{ion}^{ass} denotes the number of counterions within 7 Å from at least one network particle.

Table 3 provides the equilibrium volumes of the different systems. Regarding the single network systems, the equilibrium volume of the ref system is almost 40 times larger than that of the net1 system. It has theoretically and computationally been shown that the presence of counterions inside the gel provides a large osmotic pressure contribution, responsible

Table 3
Properties of the investigated systems

System	V[a]/Å^3 × 10^3	f_{ion}^{ass}	Polymer I			Polymer II		
			$\langle R_{ee}^2 \rangle^{1/2}$/Å	$\langle R_{bb}^2 \rangle^{1/2}$/Å	ν	$\langle R_{ee}^2 \rangle^{1/2}$/Å	$\langle R_{bb}^2 \rangle^{1/2}$/Å	ν
ref	5786 ± 50	0.53	71	5.9	0.84	–	–	–
net1	138 ± 6	–	27	5.5	0.53	–	–	–
net2	718 ± 8	0.66	33	5.8	0.78	–	–	–
ref–ref	5379 ± 18	0.57	69	5.9	0.83	69	5.9	0.83
net1–net1	215 ± 8	–	28	5.5	0.55	28	5.5	0.55
net2–net2	720 ± 8	0.73	33	5.8	0.78	33	5.8	0.78
ref–net1	1769 ± 21	0.34	49	5.7	0.72	50	5.6	0.74
ref–net2	1441 ± 8	0.70	46	5.7	0.71	41	6.0	0.87
net1–net2	485 ± 7	0.27	34	5.5	0.61	30	5.8	0.74

[a] Volume per unit cell at zero osmotic pressure. Error estimate $\sigma(\langle R_{ee}^2 \rangle^{1/2}) = 0.2$ Å.

for the generally very large swelling of polyelectrolyte gels [21,15,16]. The short-range repulsive LJ potential in the net1 system provides only a small contribution to the osmotic pressure [15,16]. The equilibrium volume of the net2 system per unit cell is smaller than the corresponding volume of the ref system mainly due to shorter chains connecting the crosslinks.

The equilibrium volumes of the systems with two interpenetrating networks are also given in Table 3. Of special interest is a comparison of these volumes with the volumes of their parent systems containing a single network. First, the equilibrium volume of the ref–ref system is 8% less than that of ref system. In the ref–ref system there are twice the number of counterions than in the ref system, which would intuitively provide twice the osmotic pressure as compared to that of the ref system. But the elastic properties of the two networks in the interpenetrating network system are operating in parallel, and therefore the system has an effective spring constant that is twice as large as that of the single network. Consequently, the doubling of the number of counterions should be balanced by the doubling of the spring constant. However, we observe that the volume of the ref–ref system is 8% smaller than that of ref system. This could be rationalized by the increase of the fraction of counterions that are associated to network chains from 53% for the ref system to 57% for the ref–ref system. Therefore, the fraction of counterions that contribute to the osmotic pressure in the ref–ref system is smaller than that in ref system. That makes these counterions osmotically less active; and hence, the volume of the interpenetrating network system becomes smaller than that of the corresponding single network system. The equilibrium volume of the net1–net1 system is larger than the volume of the net1 system. An increase of the number of particles increases the short-range repulsion between network particles, and therefore leads to an increased osmotic pressure. This is the dominating swelling contribution in the net1 and net1–net1 systems where the counterions are absent. The equilibrium volume of the net2–net2 system is the same as that of the net2 system. As for the ref network, the fraction of counterions associated to network chains in the interpenetrating network system is larger as compared to a system with only one network, leading to a relatively smaller contribution to the osmotic pressure from the counterions. However, due to the larger particle number density, an increase of it leads to a more pronounced rise of the osmotic pressure contribution from the excluded-volume interaction as compared to the ref and ref–ref systems. Obviously, the change in the counterion and hard-sphere contributions cancel each other for the net2 network.

The ref–net1 system swells much less than the ref system. This can be rationalized by the presence of the second neutral network, which doubles the strength of the gel without adding additional counterions to the system. Also the equilibrium volume of the ref–net2 system is smaller than that of the ref system but twice the volume of the net2 system. The number of counterions is increased three times as compared to the net2 system; however, the short chains of the net2 network are already strongly stretched in a single network system, which makes the swelling sublinear with respect to the number of counterions. The swelling of the net1–net2 system is in between that of the net1 and net2 systems. As for the ref–net1 system, we attribute the reduction of the volume as compared the system with the charged network only to the fact that the uncharged network shares the strain but does not add any counterions to the gel.

4.2. Structure

We shall now analyse the structure of selected systems with a single network or two interpenetrating networks as described by radial distribution functions (rdfs), chain end-to-end distances, and Flory exponents. These results were obtained from simulations with eight unit cells at zero osmotic pressure.

4.2.1. Radial distribution functions

The radial distribution function $g(r)$ provides the particle density at distance r from a given particle. It is conventionally normalized to unit at large separation at which the spatial correlations are lost, and it is zero at short separations when the excluded-volume interaction operates. Fig. 2 provides the rdfs for the ref system and the ref–ref system. Considering the system with a single network, the node–node rdf shown in Fig. 2a (dashed curve) reveals a maximum at 76 Å and another one with a shoulder at 125 Å. For an ideal diamond-like network composed of fused rings containing six nodes each, maxima are expected to appear at $\sqrt{3}(a/4)$, $\sqrt{8}(a/4)$, and $\sqrt{11}(a/4)$ where a is the length of the unit cell (see Fig. 1). With a box length $L = 359$ Å and $a = L/2$, these distances become 78, 127, and 149 Å, respectively. Thus, first maximum arises from the spatial correlation between topologically neighboring nodes and the second one from topologically next and next–next neighboring nodes. Therefore, at equilibrium with water the network is expanded, and the diamond-like network structure is clearly visible in Fig. 3a.

The node–bead rdf given in Fig. 2b (dashed curve) possesses a prominent maximum at 5.8 Å, corresponding to the beads directly bounded to a node. The second maximum at 10.2 Å corresponds to the second nearest bead in the chain. The rdf drops below unity at intermediate distances, but then peaks again at about 84 and 130 Å owing to the increased bead density around the nodes neighboring a node. The bead–bead rdf given in Fig. 2c (dashed curve) shows prominent maxima at 5.8 and 9.8 Å corresponding to the nearest and next-nearest neighboring beads, respectively. Also here a positive correlation appears at larger distances related to the node–node correlations.

Fig. 2d (dashed curve) shows the node–counterion rdf. It has a very prominent maximum at 2.2 Å due to the electrostatic attraction between network nodes and oppositely charged counterions. The rdf then quickly decays to a minimum at 61 Å, which corresponds to the central void of the six-membered ring. The maxima at 83 and 130 Å correspond to the accumulation of counterions around the nearest node and the following nodes, respectively, in the six-membered ring. The bead–counterion rdf given in Fig. 2e (dashed curve) is similar to the node–counterion rdf, but the features are somewhat smoothed out, consistent with a strong accumulation of the counterions to the network particles.

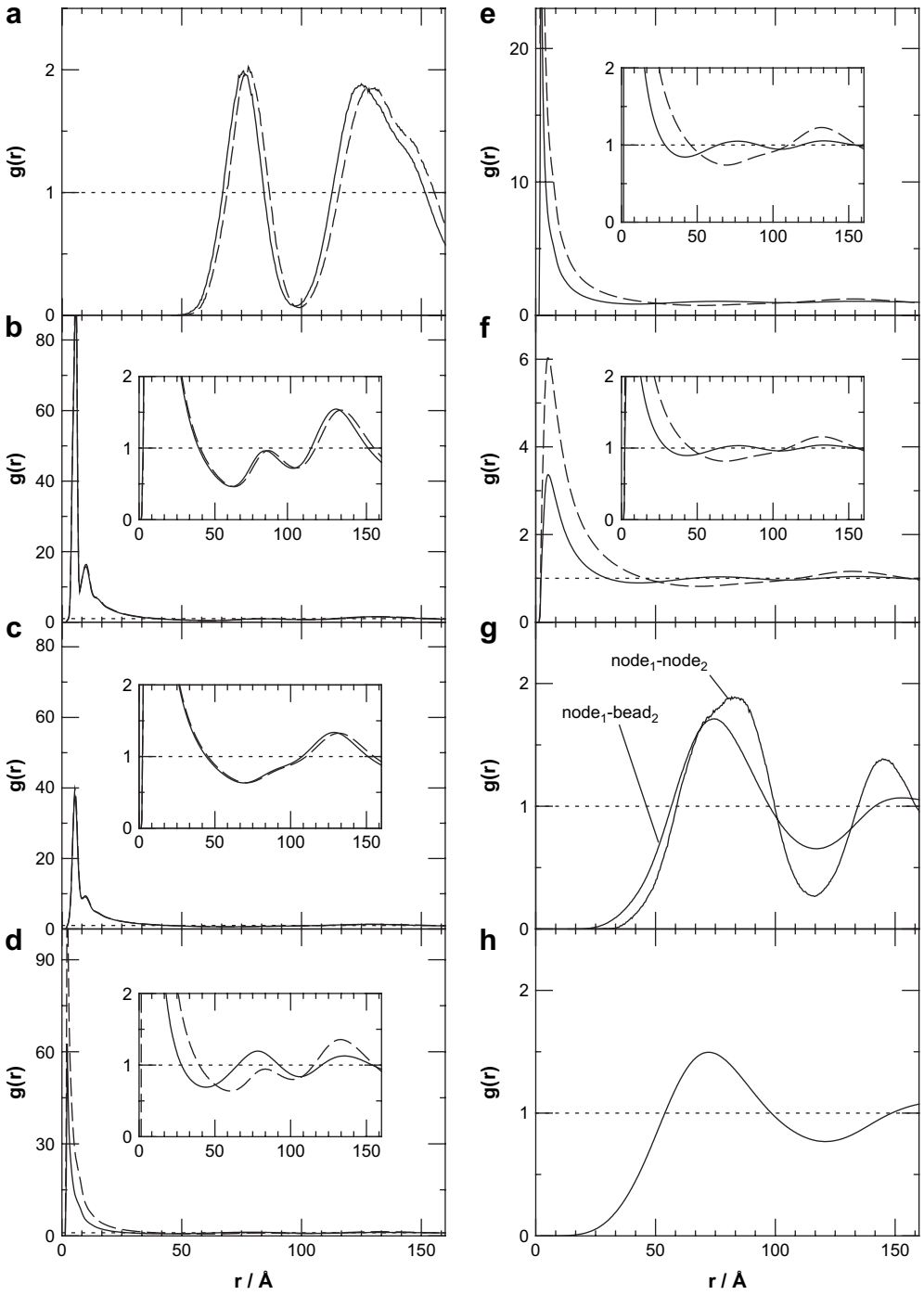

Fig. 2. (a) Node–node, (b) node–bead, (c) bead–bead, (d) node–counterion, (e) bead–counterion, (f) counterion–counterion, (g) $node_1$–$node_2$ and $node_1$–$bead_2$, and (h) $bead_1$–$bead_2$ radial distribution functions for the system with a single reference network (dashed curves) and with two interpenetrating reference networks (solid curves) obtained from simulations at zero osmotic pressure using a system comprising of eight unit cells. In (b) and (c), the two curves are nearly indistinguishable.

The counterion–counterion rdf given in Fig. 2f (dashed curve) has a maximum at 4.6 Å, which again is consistent with that most of the counterions are closely associated to the network. A minimum appears at about 68 Å and a maximum at 130 Å, again related to the spatial extension of the six-membered ring and the counterions associated to it.

We will now consider the system with the two interpenetrating networks. Panels a–c of Fig. 2 (solid curves) show that the node–node, node–bead, and bead–bead rdfs for nodes and beads residing in the *same* network are nearly identical than those of the corresponding single network system. Nevertheless, a slight shift to shorter distances is seen due to the smaller equilibrium volume of the ref–ref system as compared to the ref system.

The node–counterion, bead–counterion, and counterion–counterion rdfs shown in panels d–f (solid curves) of Fig. 2

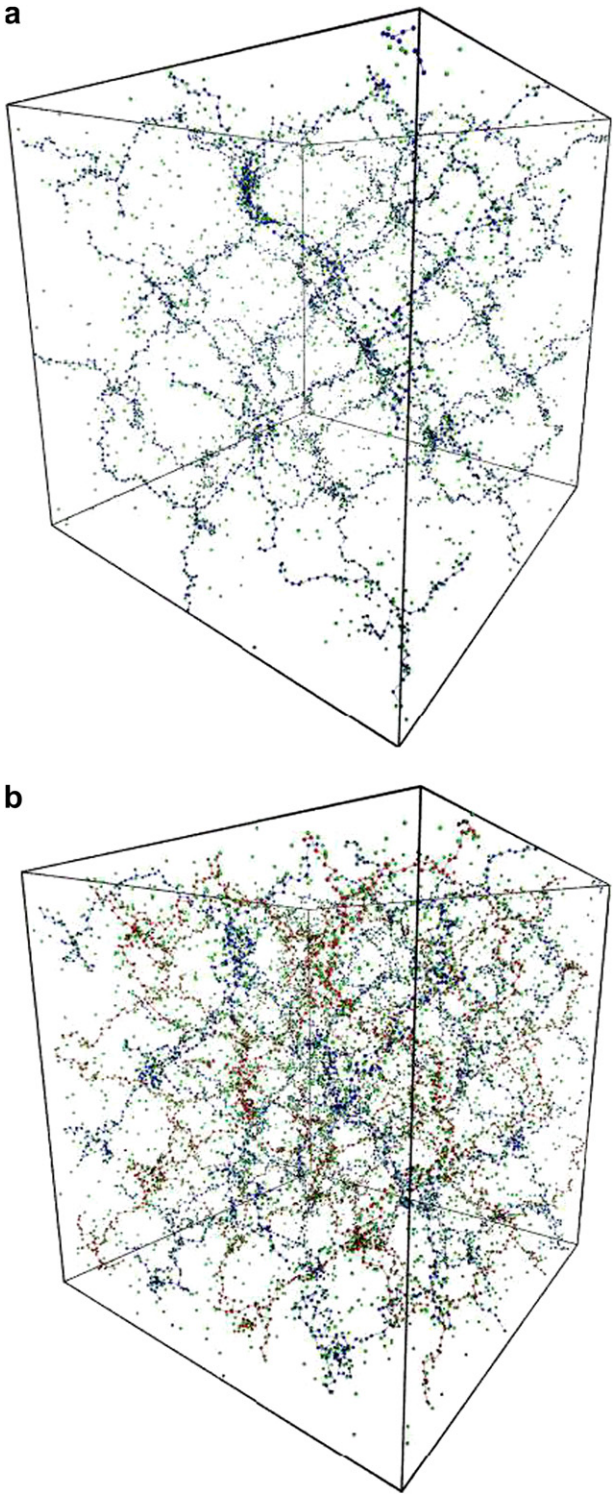

Fig. 3. Snapshots of polyelectrolyte gels at zero osmotic pressure: (a) a single network (ref system) and (b) two interpenetrating networks (the ref–ref system). Color coding: network particles (red and blue dots) and counterions (green dots). Eight unit cells are displayed. (For interpretation of the references to colour in this figure legend, the reader is referred to the web version of this article.)

have their first maximum at the same radial distance as compared to the ref system. However, before the maxima at 130 Å an additional maximum at 80 Å appears owing to the spatial correlations between, e.g., a node residing in one network and counterions associated to the other network. Hence, these additional maxima are generally due to the interpenetration of the two networks.

Panels g and h of Fig. 2 describe the rdfs for nodes and beads residing on different networks. Generally, the onset of these rdfs occurs first at 20–30 Å, showing that the two interpenetrating networks have no hard-sphere contact. Hence, the electrostatic repulsion between the two networks suppresses all molecular contact between them. The first maximum of these rdfs appears at 70–80 Å, equal to the radius of the six-membered ring, supporting evidence that one network occupies the void created by the other network. This is illustrated in Fig. 3b by an equilibrium configuration of two interpenetrating networks.

4.2.2. Chain end-to-end distance

Distribution functions of chain end-to-end distances are given in Fig. 4. Each of the panels a–c provides one distribution function for one of the three A–A type interpenetrating networks (solid curves) and a corresponding distribution function of that chain in a single network (dashed curves). Each of the other three panels provides the distribution functions of the two types of chains of the three A–B type networks (solid curves) and two corresponding distribution functions of those chains in single networks (dashed curves).

Starting with the interpenetrating networks of A–A type, the distribution functions of the end-to-end distance are similar in the interpenetrating network systems and the corresponding single network systems. Furthermore, the maxima of the distribution functions of the ref–ref, net1–net1, and net2–net2 systems are 69, 27, and 33 Å, respectively, which follow the order of the equilibrium volumes discussed in Section 4.1. A comparison of the distribution functions for chains in the interpenetrating network systems and single network systems shows that the maximum of the distribution function of the chain end-to-end distance is (i) shifted to slightly smaller value for the ref–ref system (panel a), (ii) shifted to larger value for the net1–net1 system (panel b), and (iii) the same for the net2–net2 system (panel c) as compared to the corresponding single network system. These shifts of the maxima follow qualitatively the variation of the equilibrium volume of the interpenetrating network systems and the corresponding single chain systems are also discussed in Section 4.1.

The chain end-to-end distances for the interpenetrating networks of A–B type display a more complex behavior. Starting with the ref–net1 system given in panel d, the end-to-end extensions of the charged chains in the reference network and the uncharged chains of the same length in the net1 network are virtually equal with a maximum at 50 Å. Thus, their *unequal* charge status is of no importance for their extension. This supports the notion that the intranetwork Coulomb repulsion is of marginal importance to the osmotic pressure as compared to the contribution from the counterions [16]. Obviously, the chains in the reference network become less extended and the chains in net1 network are more extended as compared to the end-to-end distances in the corresponding single network systems.

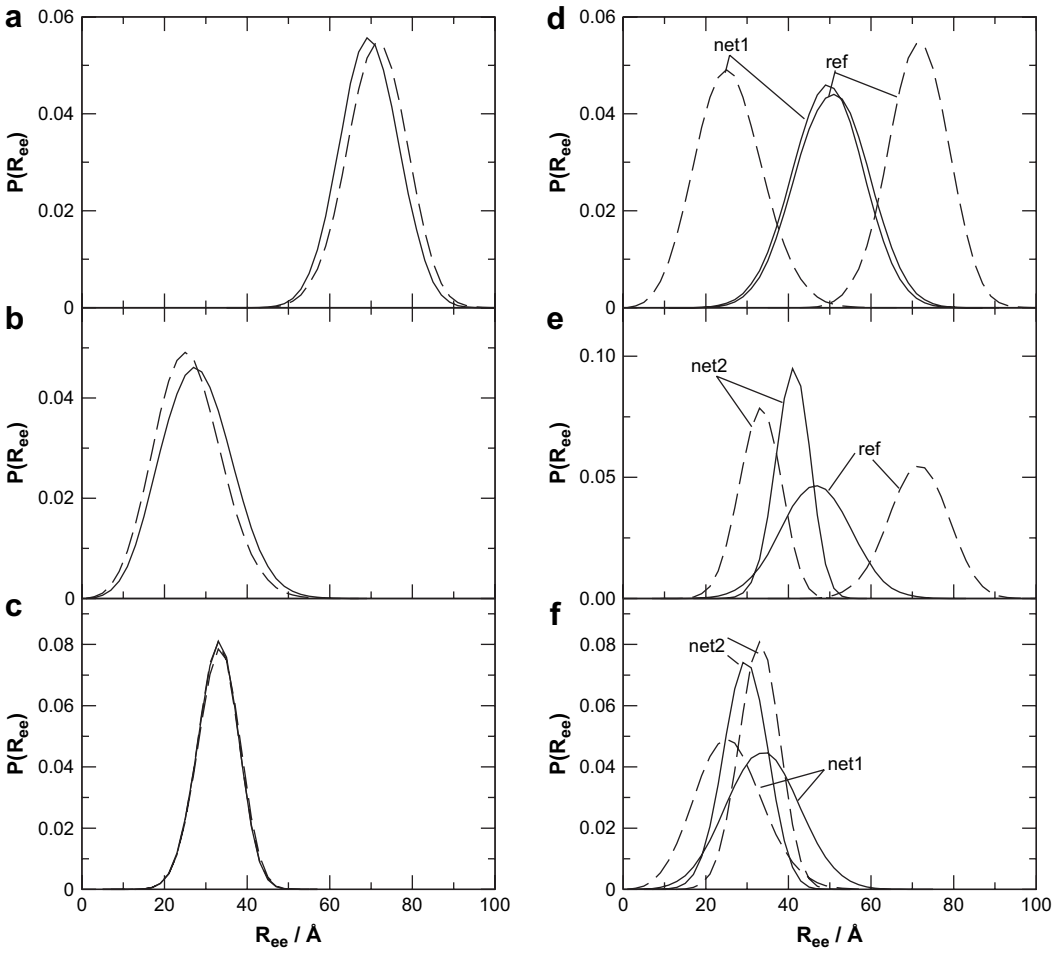

Fig. 4. Chain end-to-end distance distribution functions for the (a) ref–ref, (b) net1–net1, (c) net2–net2, (d) ref–net1, (e) ref–net2, and (f) net1–net2 interpenetrating network systems (solid curves) and corresponding distribution functions in single network systems (dashed curves) from simulations at zero osmotic pressure using systems comprising eight unit cells. In (c), the two curves are nearly indistinguishable.

Regarding the ref–net2 system shown in panel e, there is also a tendency of the two networks to have a more equal end-to-end distance as compared to the situation in the corresponding single chain networks. In this situation the chains of the two interpenetrating networks are both charged, but of different length. The distribution function of the shorter chains in net2 network (i) is much narrower and (ii) displays a maximum at somewhat shorter distance as compared to that for chains in the reference network. Thus, here the shorter chains are much more stretched. On the other hand, the extension of the longer and charged chains becomes smaller as compared to the situation in the ref system.

The most complex behavior appears when networks of differing chain length and charge status are combined (net1–net2). Panel f shows that the extension of these chains in the corresponding single chain network is fairly close, maxima at 24 Å for the net1 system containing uncharged and long chains and 33 Å for the net2 system containing charged and shorter chains. Furthermore, in the interpenetrating system the longer but more relaxed and uncharged chains in the net1 network become more stretched and the shorter but more stretched and charged chains of the net2 network become slightly less stretched. Hence, we conclude that the uncharged and longer chains in the net1 network take up some of the strain in the interpenetrating network system. Finally, we notice that the distributions of the end-to-end distances in the ref–net2 and net1–net2 systems display large similarities. The shorter charged chains in net2 network are more stretched than the longer charged chains in the ref network (panel e) or the longer uncharged chains in the net1 network (panel f). Hence, the charge status of the longer chains is of minor importance for the relative stretching of the two networks of an interpenetrating system. However, the counterions associated with the charged network give rise to an overall larger extension.

Thus, considerable differences of the chain extensions in interpenetrating networks of A–B type appear as compared to the corresponding single network systems. Generally, the enforcement of the two networks to span the same volume leads to a leveling of the extensions of the chains in the two networks. However, differences in the extensions still remain, which are due to their different chain lengths rather than a difference in charge status.

4.2.3. Flory scaling exponents

The stretching of the chains has been examined by extracting the Flory scaling exponent ν according to

$$\langle R_{ee}^2 \rangle^{1/2} = \langle R_{bb}^2 \rangle^{1/2} (n_{bead} - 1)^{\nu} \quad (5)$$

In particular, $\nu = 1/2$ for Gaussian chains and 1 for rigid rods.

The Flory scaling exponents of the chains in the ref, net1, and net2 single network systems are 0.84, 0.53, and 0.78, respectively, confirming that chains in the ref and net2 systems are strongly stretched, whereas the chains in net1 system are only weakly stretched by the excluded-volume interactions. A further examination of the Flory scaling exponents for the interpenetrating network systems confirms the conclusions made in Section 4.2.2. The strongest stretching appears for chains in net2 network in the ref–net2 system. Here, the addition of ref network to the net2 network increases the number of counterions by a factor of three, but since the length of the chains in ref network is twice that of the chains in the net2 network, most of the strain in the interpenetrating networks appears in the net2 network.

4.3. Mechanical properties

We have exerted uniaxial extension on our nine model systems and determined their responses. The box length in the z-direction was scaled according to $L_z = \lambda L$, where L is the length of the cubic box with the gel in equilibrium with pure water and λ the box extension ratio. At each λ we performed NVT simulations with varying L_x and L_y with $L_x = L_y$ to find the gel volume at which the osmotic pressure is zero. The normal stress acting on the gel was evaluated according to

$$\sigma_T = \sigma_{zz} - (\sigma_{xx} + \sigma_{yy})/2 \quad (6)$$

where $\sigma_{\alpha\alpha}$ ($\alpha = x, y, z$) are the diagonal components of the stress tensor defined according to

$$\sigma_{\alpha\alpha} = \frac{1}{V} \sum_{i=1}^{N-1} \sum_{j=i+1}^{N} \mathbf{r}_{\alpha,ij}\, \mathbf{f}_{\alpha,ij} \quad (7)$$

with $V = L_x L_y L_z$ being the volume, $\mathbf{r}_{\alpha,ij}$ the α component of the vector between particles i and j, and $\mathbf{f}_{\alpha,ij}$ the α component of the force on particle i arising from its interaction with particle j. The dependence of $\sigma_{\alpha\alpha}$ and hence σ_T on λ arises both through a variation of the forces and the cross-section areas. The response of our simulated systems to strain has been analyzed by considering the volume V and the normal stress σ_T as a function of the uniaxial strain expressed through λ. These results are given in Figs. 5 and 6, respectively.

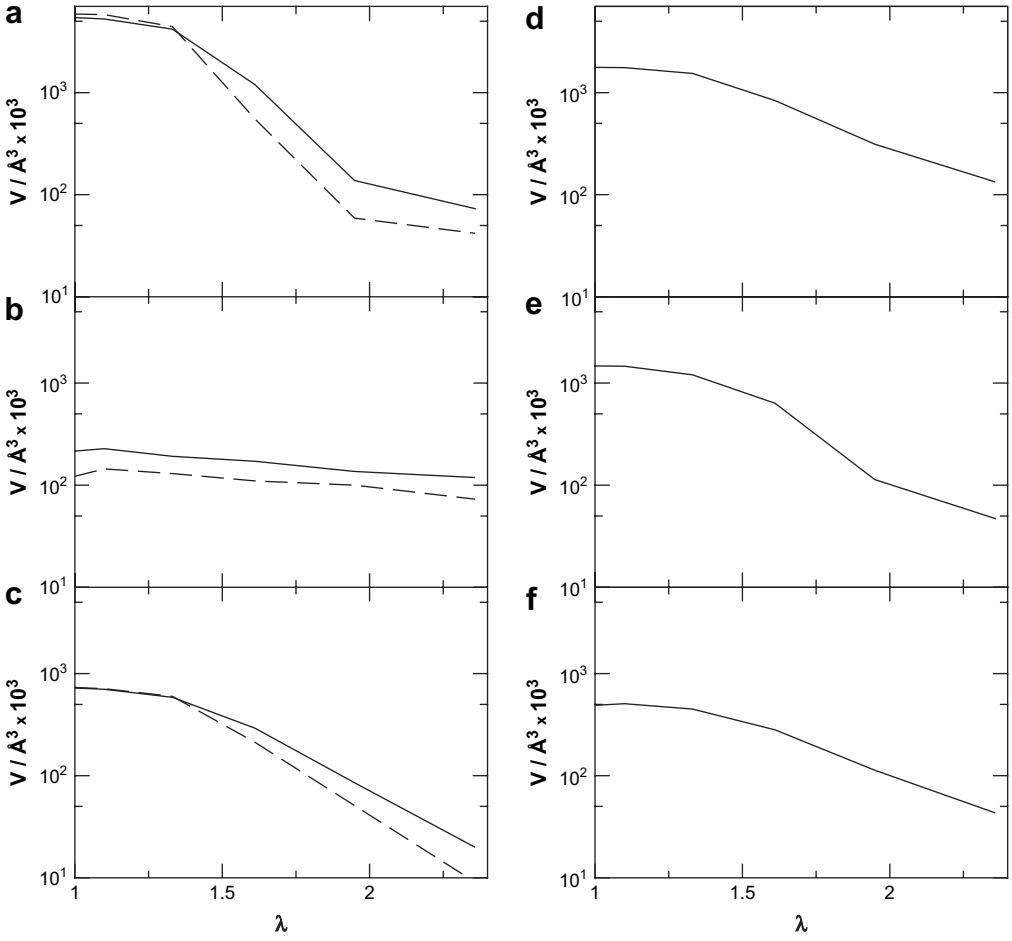

Fig. 5. Volume versus uniaxial extension ratio for the (a) ref–ref, (b) net1–net1, (c) net2–net2, (d) ref–net1, (e) ref–net2, and (f) net1–net2 interpenetrating network systems (solid curves) and corresponding single network systems (dashed curves) from simulations at zero osmotic pressure using systems comprising one unit cell.

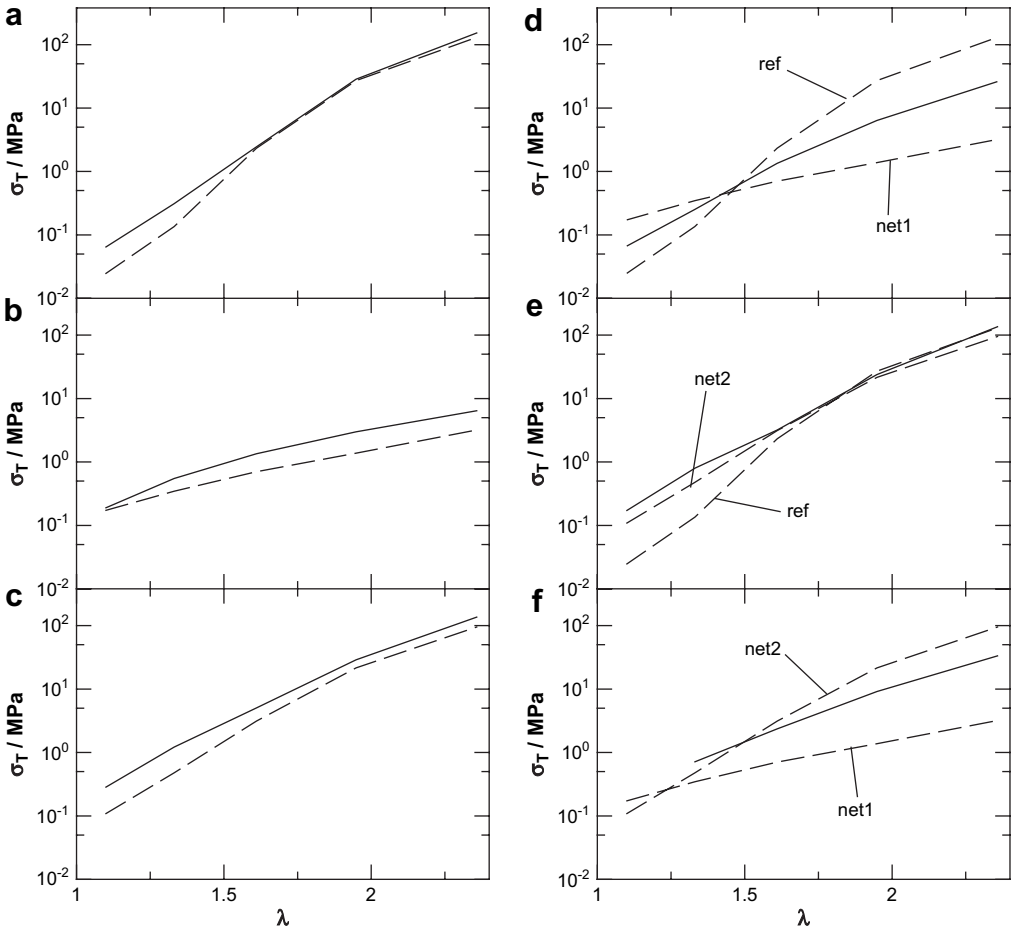

Fig. 6. Normal stress versus uniaxial extension ratio for the (a) ref–ref, (b) net1–net1, (c) net2–net2, (d) ref–net1, (e) ref–net2, and (f) net1–net2 interpenetrating network systems (solid curves), stresses in corresponding single network systems (dashed curves) from simulations at zero osmotic pressure using systems comprising one unit cell.

Fig. 5 displays that the volume of the gel decreases upon the uniaxial extension in all cases. As to the single network systems (panels a–c of Fig. 5, dashed curves), the relative volume reduction is least for the uncharged polymer network (net1) and largest for ref polyelectrolyte network. At the largest strain studied the volume decreases by factors 128, 2, and 30 for the ref, net1, and net2 systems, respectively. For interpenetrating networks of A–A type (panels a–c of Fig. 5, solid curves), the volume decrease upon strain follows qualitatively the same trend as for their single network counterparts. However, the volume reduction is less pronounced for the polyelectrolyte networks, possibly due to an increased osmotic pressure contribution from the counterions for these systems which oppose deswelling. Systems of A–B type (panels d–f of Fig. 5, solid curves) also show a pronounced volume deswelling as a function of strain, the effect being greatest for the ref–net2 system, whose volume has reduced by a factor of 38 at the largest strain observed. The net1–net2 system with fewest counterions and possessing the network with the largest crosslinking density displays the smallest volume reduction under the uniaxial extension.

We propose that the mechanism for the reduced volume upon the uniaxial extension is the following. First, the extension of the network in the z-direction creates an additional tension in the chains in the z-direction. With the topology used, all chains are oriented in a diagonal direction; hence, a reduction of the node–node extension in the x and y directions achieved by reducing L_x and L_y diminishes the increase of the tension. If the chain end-to-end separation would be conserved, geometrical arguments give that V decreases at increasing λ and becomes zero at $\lambda = \sqrt{3}$. However, such a volume reduction increases the counterion confinement and the excluded-volume repulsion, leading to a chain extension. Second, the volume response upon uniaxial stress is dependent on the network topology. For example, with a primitive-cubic lattice topology and six-functional nodes, the coupling of the network extension in the z-direction with those in the x- and y-direction becomes only indirect through the non-bonded interactions. In the present study with all chains oriented in a diagonal direction, the coupling among the three directions, and hence the volume reduction, is maximized. The volume reduction was weaker for the uncharged polymer network because their chains were not as strongly stretched as in the polyelectrolyte networks. Finally, experimentally a volume decrease upon uniaxial compression of polyelectrolyte gels has been observed [22,23]. We believe that the same underlying

mechanism is at play at both compression and extension, albeit the magnitude of the volume response generally differs.

In addition to a reduction of the gel volume, Fig. 6 shows that the normal stress increases upon an uniaxial extension. The normal stress of the three systems with a single network at low strains is not too dissimilar (panels a–c of Fig. 6), but at larger strains the stress of the ref and net2 systems becomes much larger than the stress of the net1 system. Hence, the presence of charges has a profound effect on the normal stress of these gels at large strains under the present conditions. We suggest that the much larger swelling of the polyelectrolyte gels before the uniaxial extension with the concomitant more stretched chains is the origin of the different stresses at large strains.

The normal stress of interpenetrating polyelectrolyte networks of A–A type (panels a and c of Fig. 6, solid curves) is larger than that for the corresponding single networks at low strain. We attribute this to the doubling of the network chain density and the similar gel volume. However, at larger strain the normal stress of these interpenetrating networks becomes similar to that for the corresponding single networks. Here, the larger transmitted force by the interpenetrating networks is thus balanced by their larger volume (see Fig. 5) and hence larger cross-section area. Considering the net1–net1 and net1 systems at low strain, the similar normal stress is then consistent with the twice as large volume of the net1–net1 system as compared to net1 system. The twice as large normal stress of the net1–net1 system at large strain is then qualitatively understood by the doubled network chain density and similar volume.

The stress–strain responses of the interpenetrating networks of A–B type display a rather complex behavior (panels d–f of Fig. 6, solid curves). Regarding the ref–net1 and net1–net2 systems, the most characteristic feature is that at high strains, the normal stress is that in between that of their component single networks. Hence, a synthesis of an interpenetrating polyelectrolyte network of identical or higher crosslinking density into an uncharged network leads to a toughening of the original gel, which has been experimentally observed [7]. At smaller strain, the stress of the net1–net2 system becomes much larger than that of the ref–net1 system, the reason is most likely the higher crosslinking density of the net2 network as compared to ref network. As to the ref–net2 system the stress at large strain becomes close to that of its component single networks. At small strain, the stress is similar to that of the net2 network, which is larger than that of ref network; here, the network with the larger crosslinking density dominates the stress response.

So far, we have considered gels in equilibrium with pure water. The stress–strain response upon uniaxial extension at constant gel volume will now briefly be examined. Fig. 7 shows the normal stress for the ref and net1 single networks at zero osmotic pressure and at constant volume upon uniaxial extension. For the polyelectrolyte gel, the stress increase upon extension becomes smaller at constant volume; the effect increases at increasing strain. At the largest strain, the normal stress is reduced by the factor of 100. Since the volume and hence the *xy*-cross-section area differs by about 1/100, we conclude that difference in normal stress at the two different

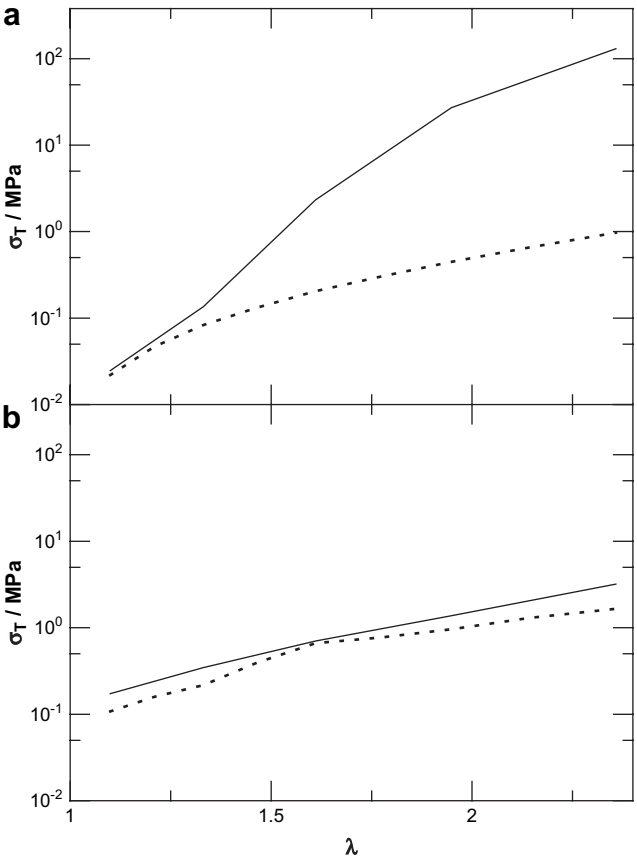

Fig. 7. Normal stress versus uniaxial extension ratio for the (a) ref and (b) net1 single network systems from simulations at zero osmotic pressure (solid curves) and at fixed volume ($V = V(\lambda = 1)$) (dotted curves) using systems comprising one unit cell.

volume conditions is mainly attributed to the different cross-section areas and less to a variation of the forces per unit cell. As to the uncharged gel, the dependence of the stress on the volume condition is much less. Here, the volume change at constant osmotic pressure was much smaller. Thus, large difference in the normal stress between polyelectrolyte and polymer gels appearing at constant osmotic pressure is strongly reduced if the uniaxial extension is made at constant volume.

We will now briefly compare the mechanical properties of some of the gels with a theory for non-Gaussian chains applicable for strongly stretched rubber [24] and highly swollen polyelectrolyte gels [25]. The non-Gaussian theory by Treloar is here modified to include (i) two interpenetrating networks (simple sum of the contributions from each network), (ii) a strain-dependent gel volume taken from our simulations, and (iii) a Flory exponent taken from our simulations (Treloar used $\nu = 1/2$ in his theory). With these modifications, we have

$$\sigma_{\mathrm{T}}^{\mathrm{theory}}(\lambda) = \frac{1}{2}\frac{k_{\mathrm{B}}T}{3V(\lambda)}\sum_{i=1}^{2} N_{\mathrm{chain},i} n_{\mathrm{bead}}^{\nu_i} \times \left[\mathcal{L}^{-1}(\lambda n_{\mathrm{bead},i}^{\nu_i - 1}) - \lambda^{-3/2}\mathcal{L}^{-1}(\lambda^{-1/2} n_{\mathrm{bead},i}^{\nu_i - 1})\right] \quad (8)$$

where $N_{\mathrm{chain},i}$ and $n_{\mathrm{bead},i}$ are the number of crosslinked chains and the number of beads in a chain, respectively, for

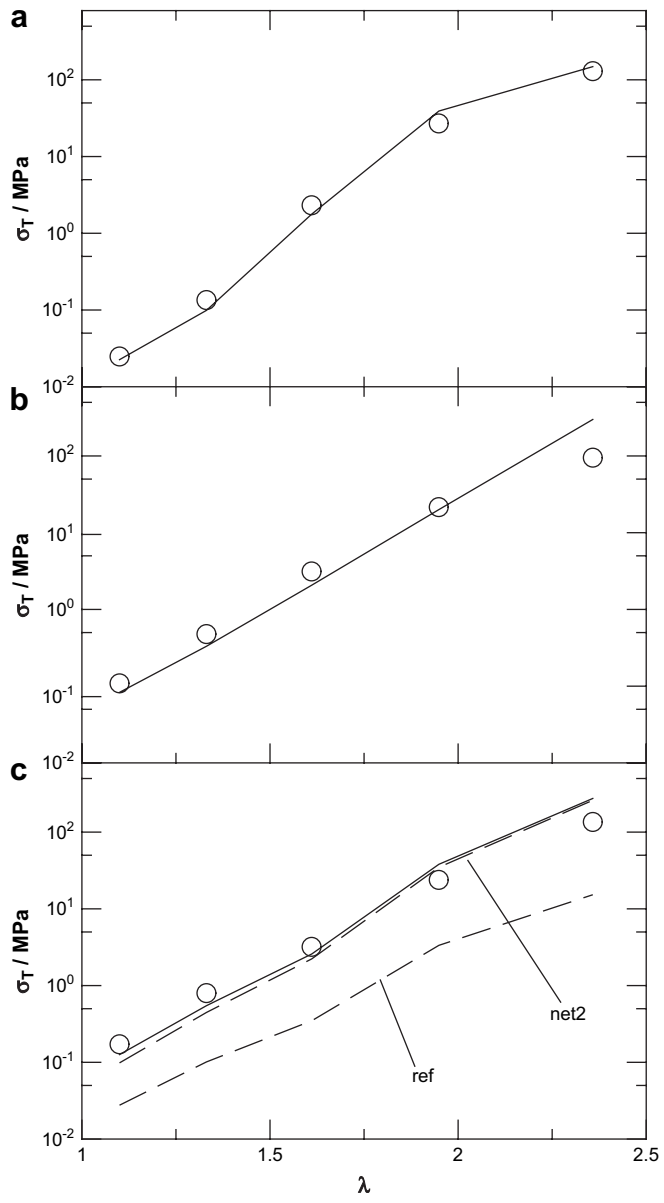

Fig. 8. Normal stress versus uniaxial extension ratio for the (a) ref, (b) net2, and (c) ref–net2 systems from simulations at zero osmotic pressure using systems comprising one unit cell (symbols) and theoretical predictions from Eq. (8) (curves). In (c), the theoretical individual network contributions are also shown (dashed curves).

network type i, $V(\lambda)$ the gel volume at the strain λ, ν_i the Flory parameter for chains of network type i at $\lambda = 1$, and $\mathcal{L}^{-1}(x)$ is the inverse Langevin function $(\mathcal{L}^{-1}(x) \approx 3x + (9/5)x^3 + (297/175)x^5 + (1539/875)x^7)$.

Fig. 8 shows the prediction of Eq. (8) (curves) with values of $V(\lambda)$, ν, and n_{bead} taken from Table 3 and Fig. 5 and the simulated results (symbols) for the ref, net2, and ref–net2 systems. A good agreement between the non-Gaussian theory and our simulated results is found for all three systems. For the interpenetrating the ref–net2 system, the theory predicts that the contribution from the chains of the net2 network is ≈ 10 times larger than that from the chains of ref network. This difference originates primarily from the stronger stretching of the shorter chains of the net2 network. At $\lambda = 1$, we had $\nu = 0.84$ and $\nu = 0.71$ for the two types of chains, respectively, see Table 3.

5. Conclusions

We have studied three single network systems and six interpenetrating network systems using Monte Carlo simulations and investigated their volume, chain properties, and mechanical properties when the gel is in equilibrium with pure water. The main conclusions of this work are as follows:

(A) (i) Interpenetrating polyelectrolyte networks of identical crosslinking density swell slightly less than the corresponding single network system. To the first order, the effect of chain and counterions per unit cell cancels each other. (ii) Interpenetrating uncharged polymer networks of identical crosslinking density swell more than the corresponding single network system. The doubling of the number of particles per unit cell gives rise to a larger excluded-volume repulsion. (iii) The swelling of interpenetrating network systems that contain both polyelectrolyte and polymer networks of different crosslinking density is insensitive which of the networks that carries the charges.

(B) When networks of low and high crosslinking densities are mixed, the shorter polymer chains become more stretched than the corresponding single network system and the longer polymer chains become less stretched than its corresponding single network system.

(C) The structure of the interpenetrating polyelectrolyte networks shows that network particles mutually repel each other and there is no molecular contact.

(D) Upon uniaxially stretching of a swollen polyelectrolyte network, the equilibrium volume decreases. The stretching of chains in the direction of extension is partly compensated by a reduction of the extension in the other two directions. The volume response is expected to be dependent on the network topology.

(E) At large strain, the charged single networks displayed a larger normal stress as compared to the uncharged network.

Acknowledgements

We thank Dave Myung and Alexei Khokhlov for fruitful discussions and the Centre for Amphiphilic Polymers (CAP) for funding.

References

[1] Gong J, Katsuyama Y, Kurokawa T, Osada Y. Adv Mater 2003;15:1155.
[2] Yasuda K, Gong JP, Katsuyama Y, Nakayama A, Tanabe Y, Kondo E, et al. Biomaterials 2005;26:4468.
[3] Na Y-H, Kurokawa T, Katsuyama Y, Tsukeshiba H, Gong JP, Osada Y, et al. Macromolecules 2004;37:5370.
[4] Nakayama A, Kakugo A, Gong JP, Osada Y, Takai M, Erata T, et al. Adv Funct Mater 2004;14:1124.

[5] Tanaka Y, Gong J, Osada Y. Prog Polym Sci 2005;30:1.
[6] Myung D, Koh K, Bakri A, Zhang F, Marshall A, Ko J, et al. Biomed Microdevices 2007;9:911.
[7] Myung D, Koh W, Ko J, Hu Y, Carrasco M, Noolandi J, et al. Polymer 2007;48:5376.
[8] Kwon H, Gong J. Curr Opin Colloid Interface Sci 2006;11:345.
[9] Myung D, Koh W, Ko J, Noolandi J, Carrasco M, Smith A, et al. Invest Ophthalmol Vis Sci 2005;46:5003.
[10] Tanaka Y. Europhys Lett 2007;78:56005.
[11] Svaneborg C, Grest GS, Everaers R. Phys Rev Lett 2004;93: 257801.
[12] Svaneborg C, Grest GS, Everaers R. Europhys Lett 2005;72:760.
[13] Everaers R. New J Phys 1999;1:12.1.
[14] Jang S, Goddard W, Kalani M. J Phys Chem B 2007;111:1729.
[15] Schneider S, Linse P. Eur Phys J 2002;8:8030.
[16] Schneider S, Linse P. J Phys Chem B 2003;107:8030.
[17] Schneider S, Linse P. Macromolecules 2004;37:3850.
[18] Edgecombe S, Schneider S, Linse P. Macromolecules 2004;37:10089.
[19] Allen MP, Tildelsley DJ. Computer simulation of liquids. Oxford University Press; 1987.
[20] Linse P. MOLSIM 4.07. Lund: Lund University; 2004.
[21] Khokhlov AR, Starodubtev SG, Vasilevskaya VV. Conformational transitions in polymer gels: theory and experiment. In: Responsive gels: volume transitions 1, vol. 109. Springer-Verlag; 1993.
[22] Budtova T, Suleimenov I. Polymer 1997;38:5947.
[23] Vervoort S, Patlazhan S, Weyts J, Budtova T. Polymer 2005;46:121.
[24] Treloar LRG. The physics of rubber elasticity; 1958.
[25] Gundogan N, Melekaslan D, Okay O. Eur Polym J 2003;39:2209.